WAVELET BASED CANCELLATION OF RESPIRATORY ARTIFACTS IN IMPEDANCE CARDIOGRAPHY

Vinod K. Pandey[1] and Prem C. Pandey[2]

[1]BME Group, Bio School, IIT Bombay, Powai Mumbai 400 076, India
[2]EE Dept., IIT Bombay, Powai Mumbai 400 076, India

ABSTRACT

Impedance cardiography is a noninvasive technique for monitoring stroke volume, based on sensing variation in the thoracic impedance, $z(t)$, due to blood flow. In this technique, first derivative of impedance, dz/dt, is used to calculate two parameters: ventricular ejection time and $(-dz/dt)_{max}$. Respiration and motion artifacts cause base line drift in the sensed impedance waveform, particularly during exercise, and this drift results in errors in the estimation of the two parameters. Ensemble averaging of dz/dt signal suppresses respiratory and motion artifacts but it introduces distortion in the signal. In this study, a wavelet based denoising method is used to cancel corrupting respiratory artifacts from the dz/dt and $z(t)$ signals in order to make a reliable estimate of cardiac output.

Index Terms— Wavelet denoising, Respiratory artifacts, Impedance cardiography.

1. INTRODUCTION

Impedance cardiography is a noninvasive technique for monitoring stroke volume, based on sensing the changes in the electrical impedance of the thorax, $z(t)$, caused by variation in blood volume during the cardiac cycle [1]-[14]. Time derivative of the thoracic impedance ($-dz/dt$) is known as impedance cardiogram (ICG). The parameters required for estimating the stroke volume, using Kubicek, Bernstein, or Sramek formulas [1]-[3] are left ventricular ejection time (T_{lvet}) and maximum change in the impedance cardiogram, $(-dz/dt)_{max}$.

Fig. 1 shows ICG and other related waveforms. Ventricular ejection time is defined as the time difference between points B and X in ICG waveform. The point B, often occurring at onset of rapid upstroke of ICG, corresponds to opening of the aortic valve. While the aortic valve closure is identified as point X, associated with the minimum following the maximum in ICG. Point X corresponds to second heart sound in phonocardiogram. Point B is generally identified as base line crossover point before maximum peak of ICG. DeMarzo and Lang [8] observed that B-point can occur at any point on the ascending segment of the waveform in some patients. Further, sensing of the variation in thoracic impedance due to blood flow is influenced by respiratory and motion artifacts [2], [5], [10], [12], [13]-[18]. These artifacts have large amplitude as compared to impedance variation due to cardiac cycle, and can cause a large base line drift. ICG signal bandwidth extends over 0.8-20 Hz. Respiration related artifacts extend over 0.04-2 Hz, while motion related artifacts have band of 0.1-10 Hz [9], [13]-[15]. Therefore spectra of the motion and respiratory artifacts may partly overlap with that of the ICG. This causes errors in detection of T_{lvet} and $(-dz/dt)_{max}$ from ICG waveform.

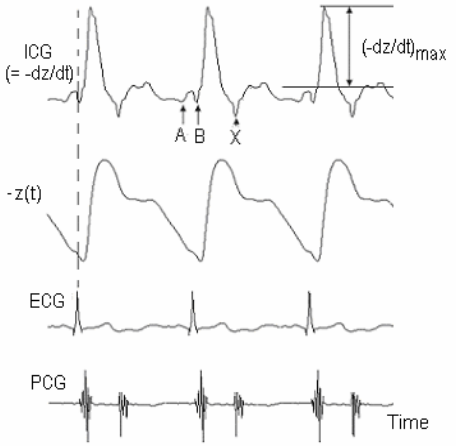

Fig. 1. Typical impedance cardiogram (adapted from [3]). $z(t) = Z(t) - Z_o$ where $Z(t)$ is thoracic impedance and Z_o is the basal impedance.

Holding the breath during recording can avoid respiratory artifacts, but it may change the stroke volume. Holding of breath is generally difficult during or after exercise. Ensemble averaging is the most commonly used technique for suppressing artifacts in the ICG signal [5], [6], [10], [13]. Ensemble averaging is carried out using time frames with an internal reference point or with respect to a reference point in another waveform. Normally, simultaneously acquired electrocardiogram (ECG) R-points are used for ensemble averaging the ICG waveform on beat-by-beat basis. However, this suppresses beat-to-beat relation and transient changes. Because of heart rate variability, ensemble averaging tends to blur or suppress the less distinctive point B of the waveform and may result in error in its detection [10], [11], [15]-[18]. Further, the time

1-4244-0882-2/07/$20.00 ©2007 IEEE

difference between B-point of ICG and R-point of ECG may change, resulting in smudging of ICG peaks.

Yamamota *et al*. [15] used a narrow bandpass IIR filter, centred around the heart rate. However, it introduces nonlinear phase distortion and attenuates high frequency components of ICG signal. Raza *et al*. [17] used a highpass IIR filter with voluntary cardio-respiratory synchronization. In this technique, the highpass cut-off frequency is varied as a function of heart rate and forward filtering followed by backward filtering is used to reduce phase distortion. The disadvantage of this technique is the possibility of distortion of the ICG signal acquired during exercise and post-exercise relaxations. Due to a partial overlap between the spectra of ICG and respiratory artifacts, non-adaptive digital filters are not effective in removal of the artifacts from ICG and $z(t)$. Barros *et al*. [18] used an adaptive filter with scaled Fourier linear combiner for removal of movement artifacts. ICG signal was expressed as a Fourier series, with a period determined by R-R interval of ECG. Pandey and Pandey [19] used a LMS based adaptive filter in which the respiratory signal, acquired from a respiratory sensor simultaneously with ICG, was used as reference input. These adaptive methods fail to cancel the artifacts if the spectral components of artifacts coincide with those of the ICG.

In this paper, a wavelet-based denoising method [20], [21] is investigated to examine the applicability of DWT (discrete wavelet transform), for cancellation of the respiratory artifacts from the recorded ICG signals. FIR based Meyer wavelet [20] has been used for decomposition of contaminated $z(t)$ and ICG signal, and the first few dilated components have been used to reconstruct the signal. This technique does not require any control of respiration.

2. METHOD

2.1 Wavelet Based Denoising Technique

Wavelet based denoising techniques have been applied in many biosignal applications [22], [23]. The wavelet transform decomposes a signal into an approximation signal and a dilated signal [20], [21]. The approximation signal is subsequently divided into new approximation and dilated signals. This process is carried out iteratively, by breaking down the signal into many lower-resolution components. In wavelet based denoising, the decomposed components corresponding to artifacts are attenuated without substantially affecting the main features of the signal [20], [21].

Different types of wavelets were used to study the decomposition of ICG into different levels. FIR based Meyer wavelet [20] captured the ICG in its first few levels and the artifacts component in the other levels for a wide variation in the cardiac and respiratory rates. Using this wavelet, the acquired signal is decomposed up to 10 levels. The wavelet coefficients are classified into: a low band where only signal components are present, a high band where only respiratory components are present, and an intermediate band with very small contribution from either. Hence, the respiratory components of the wavelet decomposition are truncated and the signal is reconstructed from the remaining components in the low band.

2.2 Experimental Set-up

Recordings were done on more than 50 volunteers (age: 21-35 years) with normal health and no known history of cardiovascular disorders. Impedance cardiograph instrument was used for recording $z(t)$, ICG, and ECG waveforms. Impedance variation was sensed by injecting a high frequency ($\approx$ 100 kHz), low intensity (<5 mA) current into the thorax. Four-electrode configuration, with disposable spot electrodes, was used for reducing the effect of skin-electrode contact impedance. In the physical arrangement of outer pair, one electrode was placed around abdomen at the lateral side of the lower ribs and the other around upper part of the neck. For the inner electrode pair, one electrode is placed around the thorax at the level of joint between xiphoid and sternum and the other around the lower part of the neck. Waveforms of the varying thoracic impedance $z(t)$, ICG, Z_o, and ECG were simultaneously acquired at a sampling rate of 500 Sa/s with 12-bit resolution using a data acquisition unit interfaced to PC through USB port. The signals were recorded for 20 s duration at 5 min. intervals in normal resting conditions and post-exercise resting condition.

2.3 Signal Analysis

The recorded $z(t)$ and ICG waveforms exhibited strong presence of respiratory artifacts, particularly in the post-exercise recordings. A FIR based Meyer wavelet has been used for 10 levels of decomposition. By using hard thresholding, the low-frequency components corresponding to respiration, which occurs above the 8th decomposition level, are set to zero. The ICG signal is reconstructed from the remaining components. Similar analysis was carried out on $z(t)$ signal. The reconstructed denoised signals show impedance related changes corresponding to blood flow related changes across thorax, hence suppressing respiration related changes.

3. RESULTS

3.1 Denoising of Signal with Simulated Artifacts

For an estimation of effectiveness of the wavelet denoising technique in removing the respiratory artifacts, a simulation was carried out for different levels of artifacts. Recorded ICG signal is composed of bioimpedance signal related to blood flow and artifacts. For artifact free ICG signal, the subject held the breath. Another recording was made with the subject synchronizing the respiration with an

external signal. The recorded waveform was ensemble averaged with respect to respiratory cycle to estimate one cycle of respiratory artifact, and cycles of this waveform were concatenated to simulate a periodic respiratory artifact. The ICG and the estimated respiratory artifact were added at different signal-to-noise ratios (SNR) to obtain contaminated ICG signals. For the performance measurement of the method, output SNR (SNR_{out}) was calculated as

$$\mathrm{SNR}_{\mathrm{out}} = 10\log\left(\sum_{i=1}^{N} s^2(n) / \sum_{i=1}^{N} (s^2(n) - \hat{s}^2(n))\right) \qquad (1)$$

where, N is the total number of samples in the signal, $s(n)$ is the artifact free input signal, and $\hat{s}(n)$ is the recovered output signal after denoising. An SNR improvement of 20 dB for the ICG and $z(t)$, were obtained for input SNR range of -6 to -9 dB.

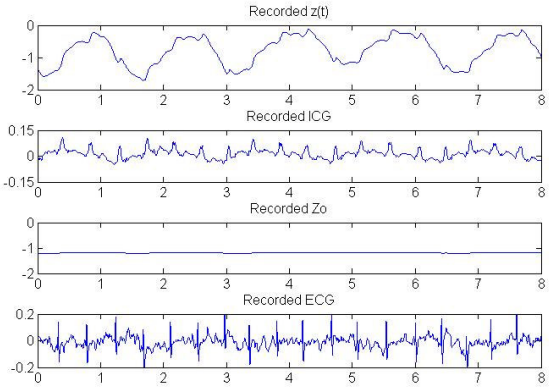

Fig. 2. Recorded $z(t)$, ICG, Z_o, and ECG from subject 'MS' in post-exercise condition (X-axis: time in s).

3.2 Denoising of Recorded Signals

Fig. 2 shows the recorded $z(n)$, ICG, Z_o, and ECG waveforms from a post-exercise recording on one of the subjects. Fig. 3 shows different levels of decomposition for ICG. Fig. 4 shows the processing results. In the acquired waveform, ICG is contaminated by respiratory artifact, making it difficult to detect T_{lvet} and ICG peaks appear to change from cycle to cycle. The second waveform in Fig. 4 is an estimate of respiratory artifacts by setting dilated coefficients below the level 9 at zero while the approximation coefficients are not altered. The third waveform is the cleaned ICG after adding dilated component from D1 to D8 of the contaminated ICG. Denoised ICG shows almost no effect of respiration, improving the detection of the B and X points. Values of ICG peaks are found to be stable. Similar analysis was carried on $z(t)$ and results of decomposition and denoising are shown in Fig. 5 and Fig. 6. The technique was tested on several recordings from subjects and similar results were obtained.

4. CONCLUSION

For attenuating respiratory artifacts present in ICG signal, a wavelet denoising based respiratory artifacts canceller is implemented. This method decomposes signal into 10 levels and the first 8 levels are used to reconstruct the signal. Advantage of this method is that it does not require any control of respiration and can be used for cancellation of respiratory artifacts, particularly during or post exercise, when cardiac activity is rapidly changing. The thoracic impedance signal, after cancellation of respiratory artifacts, may be used for beat-by-beat stroke volume calculation.

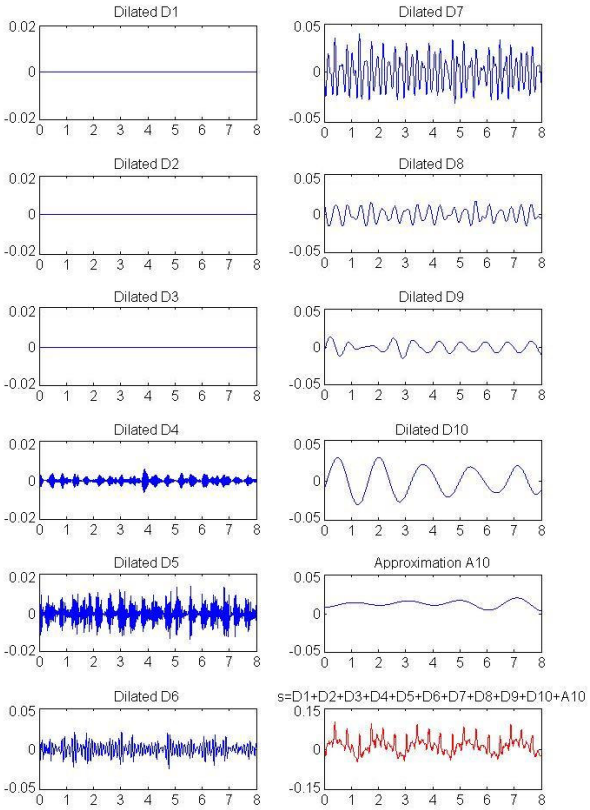

Fig. 3. Dilated and approximated levels of decomposed ICG (X-axis: time in s).

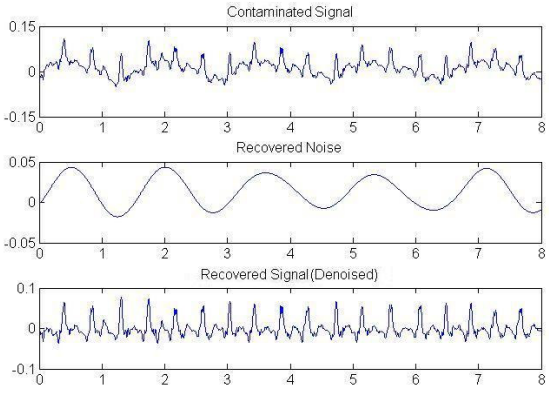

Fig. 4. Denoised output of ICG signal (X-axis: time in s).

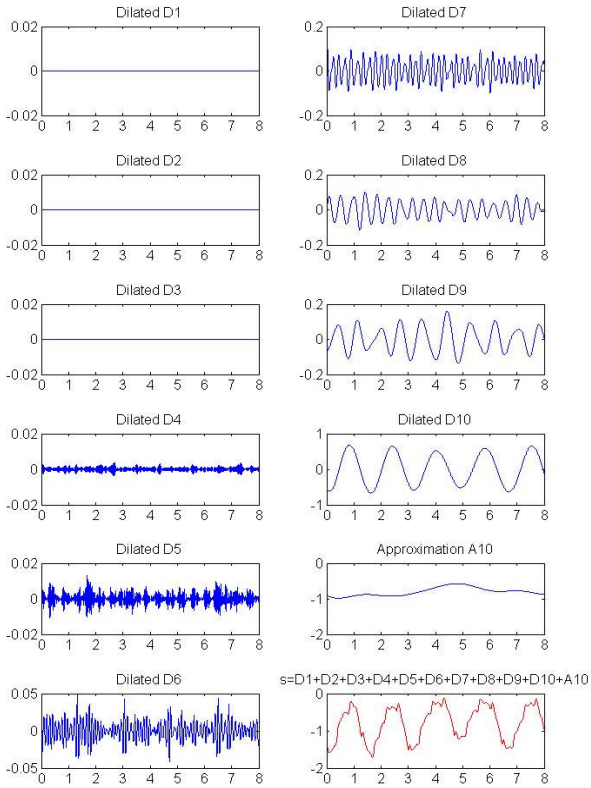

Fig. 5. Dilated and approximated levels of decomposed $z(t)$ signal (X-axis: time in s).

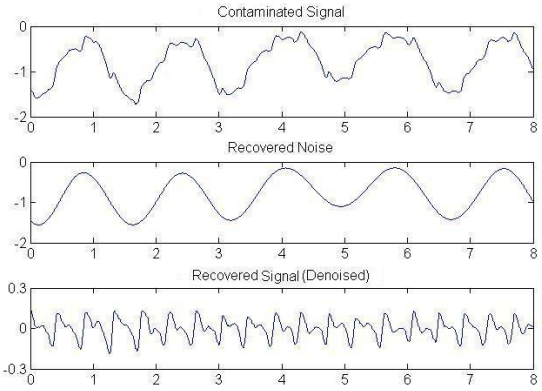

Fig. 6. Denoised output of $z(t)$ signal (X-axis: time in s).

5. REFERENCES

[1] W. G. Kubicek *et al*, "The Minnesota impedance cardiograph-theory and application," *Biomed. Eng*., vol. 9, pp. 410-417, 1974.

[2] R. P. Patterson, "Fundamental of impedance cardiography," *IEEE Eng. Med. Biol. Mag.*, vol. 8, pp. 35-38, Mar. 1989.

[3] J. Malmivuo and R. Plonsey, *Bioelectromagnetism,* Oxford Univ. Press, New York, 1995.

[4] J. Nyboer, *Electrical Impedance Plethysmography,* Charles C. Thomas, Springfield, Massachuates, 1970.

[5] M. Qu, Y. Zang, J. G. Webster, and W. J. Tompkins, "Motion artifacts from spot and band electrodes during impedance cardiography," *IEEE Trans. Biomed. Eng.,* vol. 33(11), pp. 1029-1036, Nov. 1986.

[6] Y. Zhang *et al*, "Cardiac output monitoring by impedance cardiography during treadmill exercise," *IEEE Trans. Biomed. Eng.,* vol. 33(11), pp. 1037-1041, Nov. 1986.

[7] L. E. Baker, "Principle of the impedance cardiography technique," *IEEE Eng. Med. Biol. Mag.,* vol. 8, pp. 11-15, Mar.1989.

[8] A. DeMarzo and R. M. Lang, "A new algorithm for improved detection of aortic valve opening by impedance cardiography," *Computers in Cardiology,* pp. 373-376, 1996.

[9] J. G. Webster, *Medical Instrumentation-Application and Design*, 3rd Ed., John Wiley, New York, 1998.

[10] B. E. Hurwitz *et al*, "Coherent ensemble averaging techniques for impedance cardiography," in *Proc. 3rd Annu. IEEE Symp. Comp. Based Med. Syst.*, June 1988.

[11] G. D. Jindal *et al*, "Corrected formula for estimating peripheral blood flow by impedance plethysmography," *Med. Biol. Eng. Comput.,* vol. 32, pp. 625-628, 1994.

[12] B. H. Brown *et al*, "Cardiac and respiratory related electric impedance changes in the human thorax," *IEEE Trans. Biomed. Eng.,* vol. 41(8), pp. 729-723, Aug. 1994.

[13] H. Riese *et al*, "Large-scale ensemble averaging of ambulatory impedance cardiograms," *Behavior Research Methods, Instruments, & Computers*, vol. 35(3), pp. 467-477, 2003.

[14] J. Rosell and J. G. Webster, "Signal-to-motion artifacts ratio versus frequency for impedance pneunmography," *IEEE Trans. Biomed. Eng.,* vol. 42, pp. 321-323, 1995.

[15] Y. Yamamoto *et al*, "Design and implementation for beat-by-beat impedance cardiography," *IEEE Trans. Biomed. Eng.,*vol. 35(12), pp. 1086-1090, Dec. 1988.

[16] L. Wang, R. P. Paterson, and S. B. Raza, "Respiratory effects on cardiac related impedance indices measured under voluntry cardio-respiratory synchronisation (VCRS)," *Med. Biol. Eng. Comput.,* pp. 505-510, Sept. 1991.

[17] S. B. Raza, R. P. Patterson, and L. Wang, "Filtering respiration and low-frequency movement artefacts from the cardiogenic electrical impedance signal," *Med. Biol. Eng. Comput.,* pp. 556-561, Sept. 1992

[18] A. K. Barrows, M. Yoshizawa, and Y. Yasuda, "Filtering noncorrelated noise in impedance cardiography," *IEEE Trans. Biomed. Eng.,*vol. 42(3), pp. 324-327, Mar. 1995.

[19] V. K. Pandey and P.C. Pandey, "Cancellation of respiratory artifacts in impedance cardiography," *Proc. 27th Annual Int. Conf. of the IEEE Eng. Med. Biol. Soc.* (*IEEE/ EMBC'05*), Shanghai, China, Sept. 1-4, 2005.

[20] I. Daubechies, *Ten Lectures on Wavelets*, SIAM, Philadelphia, 1992.

[21] A. N. Akansu and R. A. Haddad, *Multiresolution Signal Decomposition*, Academic Press, San Diego, 2001.

[22] H. Liang and Z. Lin, "Stimulus artifact cancellation in the serosal recordings of gastric myoelectric activity using wavelet transform," *IEEE Trans. Biomed. Eng.,* vol. 49, pp. 681-687, July 2002.

[23] S. A. Chouakri *et al*, "Wavelet denoising of the electrocardiogram signal based on the corrupted noise estimation," *Computers in Cardiology*, vol. 32, pp. 1021-1024, 2005.